Anisotropic Generalized Bayesian Coherent Point Drift for Point Set Registration

Ang Zhang, Zhe Min, Zhengyan Zhang, Xing Yang, and Max Q.-H. Meng, *Fellow, IEEE*

***Abstract*—Registration is highly demanded in many real-world scenarios such as robotics and automation. Registration is challenging partly due to the fact that the acquired data is usually noisy and has many outliers. In addition, in many practical applications, one point set (PS) usually only covers a partial region of the other PS. Thus, most existing registration algorithms cannot guarantee theoretical convergence. This article presents a novel, robust, and accurate three-dimensional (3D) rigid point set registration (PSR) method, which is achieved by generalizing the state-of-the-art (SOTA) Bayesian coherent point drift (BCPD) theory to the scenario that high-dimensional point sets (PSs) are aligned and the anisotropic positional noise is considered. The high-dimensional point sets typically consist of the positional vectors and normal vectors. On one hand, with the normal vectors, the proposed method is more robust to noise and outliers, and the point correspondences can be found more accurately. On the other hand, incorporating the registration into the BCPD framework will guarantee the algorithm's theoretical convergence. Our contributions in this article are three folds. First, the problem of rigidly aligning two general PSs with normal vectors is incorporated into a variational Bayesian inference framework, which is solved by generalizing the BCPD approach while the anisotropic positional noise is considered. Second, the updated parameters during the algorithm's iterations are given in closed-form *or* with iterative solutions. Third, extensive experiments have been done to validate the proposed approach and its significant improvements over the BCPD.**

***Note to Practitioners*—This paper was motivated by the problem of 3D rigid PSR for computer-assisted surgery (CAS), especially in orthopedic applications. The proposed algorithm is also suitable for other scenarios where the initial coarse registration is conducted. The traditional registration methods are susceptible to noise (especially anisotropic noise), outliers, and incomplete partial data. This paper generalizes the recently proposed BCPD method to the six-dimensional scenario where anisotropic positional noise is considered and normal vectors are incorporated. The proposed noise model is decomposed into three parts to be solved alternately: the membership probability of mixture distributions, the soft correspondence estimation, and the model parameters (i.e., the rotation matrix, translation vector, the covariance matrix with the anisotropic positional error, and the concentration parameter with the estimation of the normal vectors). Especially, the convergence is guaranteed at the theoretical level using the variational inference theory. The experimental results demonstrate the superiority of our algorithm on registration accuracy, convergence speed, and robustness to noise, outliers, and partial data.**

***Index Terms*—Rigid point set registration, correspondence estimation, anisotropic positional error, variational Bayesian inference.**

This project is partially supported by National Key R&D program of China with Grant No. 2019YFB1312400, Hong Kong HMRF under Grant 06171066, and Hong Kong RGC NSFC/RGC Joint Research Scheme #N_CUHK448/17 awarded to Max Q.-H. Meng. *(Ang Zhang and Zhe Min contributed equally to this work.) (Corresponding author: Max Q.-H. Meng.)*

Ang Zhang is with the Department of Electronic Engineering, The Chinese University of Hong Kong, N.T., Hong Kong SAR, China.

Zhe Min is with Centre for Medical Image Computing and Wellcome/EPSRC Centre for Interventional and Surgical Sciences, University College London, London, UK.

Zhengyan Zhang and Xing Yang are with the School of Mechanical Engineering and Automation, Harbin Institute of Technology at Shenzhen, Shenzhen, China

Max Q.-H. Meng is with the Department of Electronic and Electrical Engineering of the Southern University of Science and Technology in Shenzhen, China, on leave from the Department of Electronic Engineering, The Chinese University of Hong Kong, Hong Kong, China, and also with the Shenzhen Research Institute of the Chinese University of Hong Kong in Shenzhen, China (e-mail: max.meng@ieee.org).

I. Introduction

POINT set registration (PSR) is a fundamental research topic in robotics, computer vision [1], augmented reality (AR) and computer-assisted surgery (CAS) [2][3]. The target of PSR is to recover the misalignment or the best transformation between two point sets (PS). In robotics, the camera pose is usually estimated by minimizing the alignment error of corresponding feature points in all the collected frames, which is actually a global registration process [4]–[6]. To enable the AR technique that overlays computer-generated virtual components to the real environments, the registration that aligns the coordinate frame associated with the virtual environments to that of the real world is needed [7][8]. Medical image registration is essential when clinicians intend to analyze a pair of medical images from different times, different viewpoints, and different sensors or modalities (i.e., multi-modality registration). In CAS, registration is often utilized to map the pre-operative image space with the intra-operative patient space [9]–[11]. Registration problems can also be classified into two categories: rigid and non-rigid registrations. In the rigid registration, the transformation consists of a rotation matrix and a translation vector, and possibly a scaling factor [12]. In the non-rigid registration, the transformation can be represented with the thin-plate spline (TPS) [13] or displacement vectors [14]–[17]. In this paper, we focus on the 3D/3D rigid PSR for CAS applications. Three challenges can be summarized in the registration of real-world PSs. First, the points in two PSs have no known correspondences. Second, one PS is usually a partial region of the other PS. Third, the acquired PSs are often with noises and outliers.

A. Related Work

Registration methods can be divided into three categories: (a) Iterative closest point (ICP)-based methods. (b) probabilistic methods. (c) deep-learning-based methods.

1) ICP and Its Variants: ICP is a classical correspondence-free registration method, where two iterative steps (so called the correspondence and transformation steps) are involved [18]. In the correspondence step, the point correspondences between two PSs are estimated according to the current rigid transformation. In the transformation step, the rigid transformation is estimated with the updated point correspondences. However, the optimization in ICP is usually not convex and easily trapped into local optimization. Another problem of ICP is its slow convergence speed [19]. Moreover, classical ICP is sensitive to the quality of PSs including partial overlaps, outliers, and noises. There are variants of ICP to overcome the drawbacks. A globally optimal solution can be obtained by the branch-and-bound (BnB) algorithm [20] or the geometric analysis [4]. In [19], convergence speed is improved using the Anderson acceleration (AA) method. In addition, ℓ_p-norm minimization method [21] and a bidirectional KMPE loss [22] are used to improve the robustness with incomplete PS, noises, and outliers. The anisotropic-ICP (AICP) [23] utilizes the inhomogeneous covariance matrix to introduce the anisotropic localization error in the model. Although many attempts can improve the performance of PSR in different aspects, due to the ICP framework, the quality of registration will still be affected by the disadvantages mentioned above.

2) Probabilistic Registration Algorithms: To solve the problems of ICP-based methods, many probabilistic PSR algorithms with soft correspondences between two PSs have been proposed. Points in PS have varying degrees of membership between 0 and 1 in this class of algorithms. As one typical and well-known probabilistic algorithm, coherent point drift (CPD) [12] formulate the registration problem as a maximum likelihood (ML) problem using Gaussian Mixture Models (GMMs). The optimal solution is solved through the expectation-maximization (EM) technique. The E-step calculates the posterior of each correspondence, and the M-step refines the transformation [24]. GMM-SQFD [25] models two PSs as GMM and uses signature quadratic form distance to represent the two PSs' similarity. JRMPC [26] uses a joint model that registers multiple PSs with the isotropic assumption. Very recently, Bayesian CPD (BCPD) reformulates CPD using variational Bayesian inference (VBI) [27]. The motion coherence theory of CPD is replaced by VBI, and the problems about the convergence, parameter tuning, restricted acceleration that exists in the above algorithms are improved. BCPD also combines non-rigid and rigid cases into one algorithm. However, these probabilistic methods are not robust to noise and outliers without extra information of PSs.

3) Deep Learning-Based Methods: With the advancement of deep learning on PSs, such as DGCNN [28] and PointNet [29], a growing number of deep-learning-based PSR methods have been proposed and proven effective for a variety of PSR problems. These learning-based algorithms usually first project the PSs to high-dimensional space where keypoints are detected and features are extracted. Next, the correspondences are solved by matching keypoints, after which the optimal transformation is estimated for the best registration [30]. Deep learning techniques bring some successful and effective cases in 3D points-based tasks, but we should still recognize the limitations with learning-based methods. For example, 1) many learning-based methods take a supervised manner to train their networks (*e.g.*, PR-Net [31] and DGR [32]) which limits the scope of application, especially for real-world unlabeled PS data [33]; 2) even the SOTA learning-based methods struggle to obtain admissible inlier ratios in real-world scenarios [30]; 3) especially for the application of CAS, deep-learning-based methods cannot guarantee the desired error bounds to surgeons in both theoretical and practical aspects. On the contrary, several SOTA probabilistic algorithms can deal with the registration under different outliers rates and noise levels. Additionally, given the measurement error of the markers (*e.g.* fiducial localization error (FLE)), there exists the mature theory to accurately calculate the registration error such as Target Registration Error (TRE) [34] or Total Target Registration Error (TTRE) [35] model. Given the above analysis, we decide not to compare with deep-learning methods in this paper mainly targeted for CAS.

B. Contributions

In this paper, we significantly adapt the state-of-the-art BCPD framework to the scenario where generalized PSs are registered and anisotropic positional noise is considered. A generalized point in the generalized PSs consists of a positional vector and the corresponding normal vectors. The problem of aligning two generalized PSs is thus termed as generalized point set registration (GPSR). Our proposed registration method is thus called anisotropic generalized Bayesian coherent point drift (AGBCPD). The convergence of our proposed registration algorithm is theoretically guaranteed with the variational Bayesian framework and the method is suitable for the real-world scenarios where anisotropic positional error usually exists. The multivariate Gaussian distribution and von Mises–Fisher (vMF) distribution are utilized to form the hybrid mixture models (HMMs), which are then incorporated into the variational Bayesian framework. We have validated the proposed algorithm in both cases of full-to-full and partial-to-full registrations. Extensive results have demonstrated that our method outperforms the BCPD under different cases of outliers and noise.

To summarize, key contributions in this paper include:

1) The problem of rigidly aligning two general point sets (PSs) with normal vectors is incorporated into a variational Bayesian inference framework, which is solved by generalizing the Bayesian coherent point drift (BCPD) method while the anisotropic positional noise being considered;
2) The updated parameters used during the algorithm's iterations are given in closed-form *or* iterative solutions;
3) Extensive experiments have been done to validate the proposed approach and its significant improvements over the BCPD method.

II. Preliminaries

In this part, we will introduce the variational Bayesian inference (VBI) framework [36]. The target of VBI is to solve the latent variables, $\mathbf{Z}$, given observed data, $\mathbf{D}$. The posterior

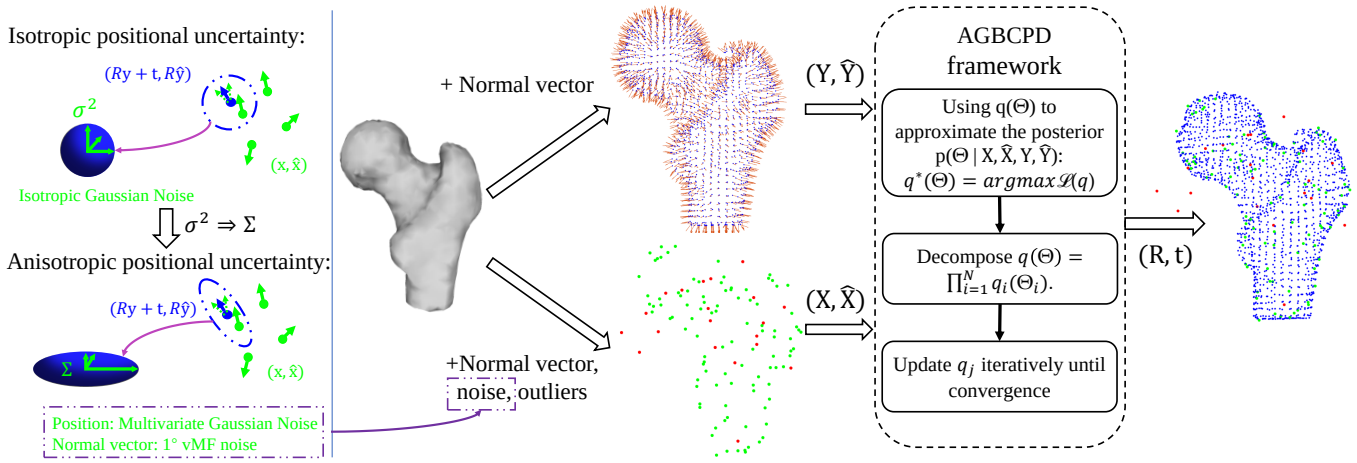

Fig. 1. The detailed process of our proposed registration framework (here we take the femur as an example). At the beginning, the bone surface is segmented from the CT volumetric images. The figure on the left illustrates the process of generating noisy target points with normals from the transformed source points with normals in scenarios of isotropic and anisotropic positional error distributions. The difference between isotropic and anisotropic scenarios is that the positional error distribution is generalized from the normal distribution (denoted as a circle in 2D) to multi-variate Gaussian distribution (denoted as an ellipse in 3D). Blue and green dots denote the positional vectors of the transformed source point set (PS) and the target PS respectively. The blue and green solid arrows represent the normal vectors of transformed source and target PS respectively. The dashed green arrows signify the sampled normals from the central normal (i.e., the normals with the transformed source PSs) in the von-Mises Fisher (vMF) distribution. In the middle, the 3D model PS $(\mathbf{Y}, \widehat{\mathbf{Y}})$ representing the bone surface is extracted from the CT images. The normal vectors are further estimated from $(\mathbf{Y}, \widehat{\mathbf{Y}})$ with PlanePCA technique. The target point set $(\mathbf{X}, \widehat{\mathbf{X}})$ is corrupted with anisotropic positional noise, vMF noise, and outliers (denoted as red dots). On the right, we show that the positional vectors together with the normal vectors in two spaces are taken as inputs for the anisotropic generalized Bayesian coherent point drift (AGBCPD) algorithm. The rotation matrix and translation vector are estimated after the optimization process.

distribution $p(\mathbf{Z}|\mathbf{D})$ or the expectation $E[\mathbf{Z}]$ over $p(\mathbf{Z}|\mathbf{D})$ is the first necessary step. Nevertheless, it is always unfeasible in actual applications because of the difficult calculation of the posterior. VBI can relax the computational complexity as an approximation method. The true posterior $p(\mathbf{Z}|\mathbf{D})$ is replaced by a tractable distribution $q(\mathbf{Z})$. Generally, the marginal probability of the model evidence $p(\mathbf{D})$ is defined as follows:

$$\ln p(\mathbf{D}) = \underbrace{\int q(\mathbf{Z}) \ln \left\{ \frac{p(\mathbf{D}, \mathbf{Z})}{q(\mathbf{Z})} \right\} \mathrm{d}\mathbf{Z}}_{\mathcal{L}(q)} - \underbrace{\int q(\mathbf{Z}) \ln \left\{ \frac{p(\mathbf{Z} \mid \mathbf{D})}{q(\mathbf{Z})} \right\} \mathrm{d}\mathbf{Z}}_{\mathrm{KL}(q \| p)} \quad (1)$$

VBI is the minimization of the KL divergence above. It can also be regarded as maximizing the evidence lower bound (ELBO) $\mathcal{L}(q)$. To solve the optimization problem, $q(\mathbf{Z})$ is decomposed as $\prod_{i=1}^{N} q_i(\mathbf{Z}_i)$, where each $\mathbf{Z}_i$ is mutually independent. Then, the general solution of the posterior approximate distribution $q_j^\star(\mathbf{Z}_j)$ can be solved as:

$$\ln q_j^\star(\mathbf{Z}_j) = E_{i \neq j}[\ln p(\mathbf{D}, \mathbf{Z})] + const, \quad (2)$$

where $E_{i \neq j}[\ln p(\mathbf{D}, \mathbf{Z})] = \int \ln p(\mathbf{D}, \mathbf{Z}) \prod_{i(\neq j)}^{N} q_i \, \mathrm{d}\mathbf{Z}_i$ and the constant term can be derived by normalizing the $q_j^\star(\mathbf{Z}_j)$. The coordinate ascent algorithm is adopted to update q_j, which guarantees monotonically increasing of ELBO and the convergence of VBI.

III. Methods

A. Problem Formulation

In the PSR problem, we aim to align together two PSs $\mathbf{X}=\{\mathbf{x}_n\}_{n=1}^{N}$ and $\mathbf{Y}=\{\mathbf{y}_m\}_{m=1}^{M}$ and corresponding unit normal vector sets $\widehat{\mathbf{X}}=\{\widehat{\mathbf{x}}_n\}_{n=1}^{N}$, $\widehat{\mathbf{Y}}=\{\widehat{\mathbf{y}}_m\}_{m=1}^{M}$ with $\mathbf{x}_n, \mathbf{y}_m, \widehat{\mathbf{x}}_n, \widehat{\mathbf{y}}_m \in \mathbb{R}^3$. On one hand, the points in $\mathbf{Y}$ are considered as the centroids of the Gaussian Mixture Model (GMM) while the mean directions of the Fisher Mixture Model (FMM) is represented as the unit normal vectors from $\widehat{\mathbf{Y}}$. On the other hand, the points in the target PS $\mathbf{X}$ and normal vectors in the normal vector set $\widehat{\mathbf{X}}$ are assumed to be generated from the GMM and the FMM respectively. The final goal of PSR is to solve the optimal rigid transformation matrix between $(\mathbf{X}, \widehat{\mathbf{X}})$ and $(\mathbf{Y}, \widehat{\mathbf{Y}})$. Under the framework of the hybrid mixture model (HMM), the probability density function (PDF) of $\mathbf{x}_n$ given $v_n = m$ (where $v = \{v_n\}_n^N$ is an index vector that nth observed point $\mathbf{x}_n$ belongs to the mth HMM component $\mathbf{y}_m$) is defined as follows:

$$\begin{aligned} p(\mathbf{x}_n, \widehat{\mathbf{x}}_n \mid v_n = m; \mathbf{R}, \mathbf{t}, \mathbf{\Sigma}, \kappa) &= \mathcal{N}(\boldsymbol{\mu}_p, \mathbf{\Sigma}) \cdot \mathcal{F}(\widehat{\boldsymbol{\mu}}_o, \kappa) = \\ &\underbrace{\frac{1}{\sqrt{(2\pi)^3 |\mathbf{\Sigma}|}} e^{-\frac{1}{2}(\mathbf{x}_n - \mu_p)^\top \mathbf{\Sigma}^{-1}(\mathbf{x}_n - \mu_p)}}_{\text{Multivariate Gaussian Distribution}} \cdot \underbrace{\frac{\kappa}{2\pi(e^\kappa - e^{-\kappa})} e^{\kappa(\mathbf{R}\widehat{\mathbf{y}}_m)^\top \widehat{\mathbf{x}}_n}}_{\text{Modified vMF Distribution}} \\ &= \frac{\kappa}{2\pi(e^\kappa - e^{-\kappa}) \cdot (2\pi)^{\frac{3}{2}} |\mathbf{\Sigma}|^{\frac{1}{2}}} e^{\kappa(\mathbf{R}\widehat{\mathbf{y}}_m)^\top \widehat{\mathbf{x}}_n - \frac{1}{2}(\mathbf{x}_n - \mu_p)^\top \mathbf{\Sigma}^{-1}(\mathbf{x}_n - \mu_p)} \end{aligned} \quad (3)$$

where $\mathbf{\Sigma}$ is the covariance matrix of multivariate Gaussian distribution, κ is the concentration parameter of the vMF distribution, $\mu_p = \mathbf{R}\mathbf{y}_\mathbf{m} + \mathbf{t}$ and $\widehat{\mu}_o = \mathbf{R}\widehat{\mathbf{y}}_m$. We denote φ_{mn} as a symbol of Eq. (3). The outliers are defined as a uniform distribution $p_{out}(\mathbf{x}_n) = 1/V$ to satisfy the normalization condition of $p_{out}(\mathbf{x}_n)$, where V is the minimum volume that can contain the whole $\mathbf{X}$. ω represents the weight of this uniform distribution, where $\omega \in [0, 1]$. We introduce $c = \{c_n\}_n^N$ as an indicator vector, which means $c_n = 1$ if the nth point in $\mathbf{X}$ is an inlier, otherwise equals 0. We use an explicit definition $\delta_m(v_n)$ to indicate the correspondence where if $v_n = m$, $\delta_m(v_n)$ is 1, otherwise 0. Moreover, we

denote $\alpha = \{\alpha_m\}_m^M \in [0,1]^M$ as the membership probabilities ($\sum_{m=1}^M \alpha_m = 1$) which represents the mixing proportion of HMM components.

Then, the joint PDF of $p(\mathbf{x}_n, \widehat{\mathbf{x}}_n, c_n, v_n)$ given $(\mathbf{Y}, \widehat{\mathbf{Y}}, \alpha, \mathbf{R}, \mathbf{t}, \mathbf{\Sigma}, \kappa)$ can be formulated as:

$$\begin{aligned} &p\left(\mathbf{x}_n, \widehat{\mathbf{x}}_n, v_n, c_n \mid \mathbf{Y}, \widehat{\mathbf{Y}}, \alpha, \mathbf{R}, \mathbf{t}, \mathbf{\Sigma}, \kappa\right) \\ &= \left\{\omega p_{\text{out}}\left(\mathbf{x}_n\right)\right\}^{1-c_n} \left\{(1-\omega)\prod_{m=1}^M \left(\alpha_m \varphi_{mn}\right)^{\delta_m(v_n)}\right\}^{c_n} \end{aligned} \tag{4}$$

which consists of two mixture distributions, the left item has two components, and the right item has M components. Denote Θ as the set of $\{\alpha, c, v, \mathbf{R}, \mathbf{t}, \mathbf{\Sigma}, \kappa\}$.

Next, we will describe in detail the method to obtain the optimal parameters $\mathbf{R}, \mathbf{t}, \mathbf{\Sigma}, \kappa$ using VBI. The general concept of our AGBCPD framework is given in Fig. 1.

B. Variational Bayesian Formulation

Under the VBI framework, the goal is to solve a distribution $q(\Theta)$ to approximate the true posterior distribution $p(\Theta|\mathbf{X}, \widehat{\mathbf{X}}, \mathbf{Y}, \widehat{\mathbf{Y}})$. At first, we define the prior distribution over the items in Θ and the joint probability distribution to formulate the variational solution of HMM.

1) Prior Distribution: We introduce a Dirichlet distribution over the membership probabilities α as:

$$p(\alpha) = \mathbf{Dir}(\alpha \mid \lambda \mathbf{1}_M) = C(\lambda \mathbf{1}_M) \prod_{m=1}^M \alpha_m^{\lambda-1},$$

where $C(\lambda \mathbf{1}_M)$ is the normalization constant and $\mathbf{1}_M$ is a column vector of all ones with size M. The Dirichlet distribution can manage the mixture proportion of HMM components. With smaller λ, the prior will affect less on the posterior, while the data will bring more influence on the posterior. To reduce the variational model, the priors over $(\mathbf{Y}, \widehat{\mathbf{Y}})$, $\mathbf{\Sigma}$, κ, and $\mathbf{R}, \mathbf{t}$ are not introduced.

2) Joint Probability Distribution: Combining the prior distribution into the HMM, the full joint probability distribution is formulated as:

$$\begin{aligned} &p(\mathbf{X}, \widehat{\mathbf{X}}, \mathbf{Y}, \widehat{\mathbf{Y}}, \Theta) \propto \\ &\qquad p(\alpha) \prod_{n=1}^N p\left(\mathbf{x}_n, \widehat{\mathbf{x}}_n, c_n, v_n \mid \mathbf{Y}, \widehat{\mathbf{Y}}, \alpha, \mathbf{R}, \mathbf{t}, \mathbf{\Sigma}, \kappa\right) \end{aligned} \tag{5}$$

C. Variational Bayesian Approximate Posteriors

We derive the approximated posterior distributions based on the VBI in this part. With the mean field theory and the conditional independence relation between variables, we factorize $q(\Theta)$ as:

$$q(\Theta) = q_1(\alpha) q_2(c, v) q_3(\mathbf{R}, \mathbf{t}, \mathbf{\Sigma}, \kappa). \tag{6}$$

which guarantees a computable solution in our Bayesian HMM. $q(\Theta)$ is updated in each iteration.

1) $q_1(\alpha)$:

The optimal $q_1^\star(\alpha)$ can be obtained using the solution (2) and the product rule for probabilities as follows:

$$\ln q_1^\star(\alpha) = E_{q_2, q_3}[\ln p(\mathbf{X}, \widehat{\mathbf{X}}, \mathbf{Y}, \widehat{\mathbf{Y}}, \Theta)] + const.$$

Substituting the full joint probability distribution (5) into the $\ln q_1^\star(\alpha)$ above and removing the terms that don't depend on α into the normalization constant, we obtain

$$\begin{aligned} \ln q_1^\star(\alpha) &= \sum_{n=1}^N \sum_{m=1}^M E_{q_2, q_3}[c_n \delta_m(v_n) \ln(\alpha_m \varphi_{mn})] \\ &+ \sum_{m=1}^M \ln \alpha_m^{\lambda-1} + const = \sum_{m=1}^M \ln \alpha_m^{\lambda-1+\rho_m} + const, \end{aligned} \tag{7}$$

where $\rho_m = \sum_{n=1}^N p_{mn}$, and $p_{mn} = E[c_n \delta_m(v_n)]$ which defines the posterior that $\mathbf{x}_n$ corresponds to $\mathbf{y}_m$. Taking the exponential of the equation above, we can solve $q_1^\star(\alpha)$ as:

$$q_1^\star(\alpha) = \mathbf{Dir}(\alpha \mid \lambda \mathbf{1}_M + \rho) \tag{8}$$

where $\rho = \mathbf{P}\mathbf{1}_N$, and $\mathbf{P} = (p_{mn}) \in \mathbb{R}^{M \times N}$ is the probability matrix. It also follows a Dirichlet distribution.

2) $q_2(c, v)$:

In this part, we solve the optimal solution of $q_2(c, v)$ which represents the shape correspondence between two PSs. Similar to the previous using the general solution (2), the optimal $q_2^\star(c, v)$ can be obtained as follows:

$$\begin{aligned} \ln q_2^\star(c, v) = \sum_{n=1}^N \Bigg[&\sum_{m=1}^M \ln \left\{(1-\omega)\left\langle \alpha_m \right\rangle \left\langle \varphi_{mn} \right\rangle\right\}^{c_n \delta_m(v_n)} \\ &+ \ln \left\{\omega p_{\text{out}}\left(\mathbf{x}_n\right)\right\}^{(1-c_n)} \Bigg] + const, \end{aligned} \tag{9}$$

where $\langle \bullet \rangle$ is the operator $\exp(E[\ln \bullet])$. Using the standard solution of the Dirichlet distribution q_1, we obtain:

$$\left\langle \alpha_m \right\rangle = exp[\psi(\lambda + \rho_m) - \psi(\lambda M + N_{\mathbf{p}})], \tag{10}$$

where $N_{\mathbf{p}} = \sum_{n=1}^N \sum_{m=1}^M p_{mn}$ and $\psi(\cdot)$ is the digamma function. Because we only consider the rigid registration in this paper, then we have

$$\left\langle \varphi_{mn} \right\rangle = \varphi_{mn}. \tag{11}$$

Observing Eq. (9), we can rewrite $q_2^\star(c, v)$ in this form $q_2^\star(c, v) = \prod_{n=1}^N q_2^{\star(n)}(c_n, v_n)$, where $q_2^{\star(n)}(c_n, v_n) \propto \left\{\omega p_{\text{out}}\left(\mathbf{x}_n\right)\right\}^{(1-c_n)} \prod_{m=1}^M \left\{(1-\omega)\left\langle \alpha_m \right\rangle \left\langle \varphi_{mn} \right\rangle\right\}^{c_n \delta_m(v_n)}$. In one pair of (v_n, c_n), only one component is available. C is a normalization constant which is defined as the sum of all components $q_2^{\star(n)}(c_n, v_n)$. It can be represented as $C = (1-\omega)\sum_{m=1}^M \left\langle \alpha_m \right\rangle \left\langle \varphi_{mn} \right\rangle + \omega p_{\text{out}}\left(\mathbf{x}_n\right)$. Finally, we can express the optimal solution to $q_2^\star(c, e)$ in closed form:

$$q_2^\star(c, v) = \prod_{n=1}^N \left(1 - \rho_n'\right)^{1-c_n} \left\{\rho_n' \prod_{m=1}^M \left(\frac{p_{mn}}{\rho_n'}\right)^{\delta_m(v_n)}\right\}^{c_n}, \tag{12}$$

where $\rho_n' = \sum_{m=1}^M p_{mn}$ is the posterior that $\mathbf{x}_n$ belongs to a non-outlier, and $\rho' = \mathbf{P}^T \mathbf{1}_M$. Furthermore, $q_2^\star$ consists

of a categorical distribution and a Bernoulli distribution. The posterior probability p_{mn} is computed as follows:

$$p_{mn} = \frac{(1-\omega)\left\langle \alpha_m \right\rangle \left\langle \varphi_{mn} \right\rangle}{\omega p_{\text{out}}\left(x_n\right) + (1-\omega)\sum_{m=1}^{M}\left\langle \alpha_m \right\rangle \left\langle \varphi_{mn} \right\rangle}. \tag{13}$$

which is the fuzzy correspondence probability between $\mathbf{x}_n$ and $\mathbf{y}_m$. It is united with the previous definition because $p_{mn} = q_2^{\star(n)}(c_n, v_n) = E[c_n \delta_m(v_n)]$. This part ensures that the update of $\mathbf{P}$ with the Eq. (13) improves the lower bound.

3) $q_3(\mathbf{R}, \mathbf{t}, \mathbf{\Sigma}, \kappa)$:

The solutions of q_1 and q_2 are solved using the VBI methods. In these two parts, p_{mn} and related terms will be updated, which is analogous to the E-step of the EM algorithm. In this part, different from previous methods, we assume q_3 as a Dirac delta function [37] which means that q_3 is only described by its mode. Therefore, we directly maximize the ELBO $\mathcal{L}(q)$ to derive the closed-form solution of q_3 instead of using the VBI's general solution (2). The variational optimization of this part can be regarded as the M-step of the EM algorithm. Given $q_1(\alpha)$ and $q_2(c, v)$, we have:

$$\begin{aligned}\mathcal{L}(q) = \\ \int q_3 \cdot E_{q_1,q_2}[\ln p(\mathbf{X}, \widehat{\mathbf{X}}, \mathbf{Y}, \widehat{\mathbf{Y}}, \Theta)] d(\mathbf{R}, \mathbf{t}, \mathbf{\Sigma}, \kappa) + const.\end{aligned} \tag{14}$$

The derivation can be found in the appendix. Denote $\mathbf{F}(\Theta)$ as the expectation of the log of the joint probability distribution. Then this optimization problem [36] is reduced to maximize $\mathbf{F}(\Theta)$:

$$\begin{aligned}\mathbf{F}(\Theta) &= E_{q_1,q_2}[\ln p(\mathbf{X}, \widehat{\mathbf{X}}, \mathbf{Y}, \widehat{\mathbf{Y}}, \Theta)] = \\ &-\frac{1}{2} N_{\mathbf{P}} \log |\mathbf{\Sigma}| - N_{\mathbf{P}} \log\left(e^{\kappa} - e^{-\kappa}\right) + N_{\mathbf{P}} \log \kappa \\ &-\sum_{n=1}^{N}\sum_{m=1}^{M} p_{mn}\left(\frac{1}{2}(\mathbf{x}_n - \mu_p)^{\top}\mathbf{\Sigma}^{-1}(\mathbf{x}_n - \mu_p)\right. \\ &\left.-\kappa\left(\left(\mathbf{R}\widehat{\mathbf{y}}_m\right)^{\mathrm{T}}\widehat{\mathbf{x}}_n\right)\right) + const.\end{aligned} \tag{15}$$

where $\mu_p = \mathbf{R}\mathbf{y}_{\mathbf{m}} + \mathbf{t}$. To maximize the ELBO concerning $\mathbf{R}, \mathbf{t}, \mathbf{\Sigma}$ and κ, the first step is to update the transformation $[\mathbf{R}, \mathbf{t}]$ given current $\mathbf{\Sigma}, \kappa$ and p_{mn} with the constraint $\mathbf{R} \in SO(3)$. Denote $[\widetilde{\mathbf{R}}, \widetilde{\mathbf{t}}]$ as the transformation between two consecutive updates of q_3 part. Then we adopt Rodrigues' rotation formula, which can use a tri-vector $\theta = [\theta_1, \theta_2, \theta_3]^{\top}$ to denote a rotation $\mathbf{R}(\theta) \in SO(3)$ as follows:

$$\mathbf{R}(\theta) = \mathbf{I} + \frac{[\theta]_{\times}}{\|\theta\|}\sin(\|\theta\|) + \frac{[\theta]_{\times}^2}{\|\theta\|^2}(1 - \cos(\|\theta\|)) \tag{16}$$

where $[\theta]_{\times}$ is a 3×3 skew-symmetric matrix. Then, we can reformulate the transformation $[\widetilde{\mathbf{R}}, \widetilde{\mathbf{t}}]$ as a vecter $\boldsymbol{\xi} = [\widetilde{\theta}; \widetilde{\mathbf{t}}]_{6\times 1}$, where $\widetilde{\mathbf{R}} = \mathbf{R}(\widetilde{\theta})$. Removing the terms that are independent of $[\mathbf{R}, \mathbf{t}]$ in (15), the problem that maximizes Eq. (15) can be rewritten as an *unconstrained* optimization problem $\min_{\boldsymbol{\xi}} \mathbf{Q}(\Theta)$, whose detailed form is obtained as follows:

$$\begin{aligned}\min_{\boldsymbol{\xi}} \sum_{n=1}^{N}\sum_{m=1}^{M}\Bigg(&\underbrace{\frac{1}{2} p_{mn}^{i}(\mathbf{x}_n - \mu_p^{i})^{\top}\mathbf{\Sigma}^{i-1^{-1}}(\mathbf{x}_n - \mu_p^{i})}_{\mathbf{Q}_{P,mn}^{i}} \\ &\underbrace{-p_{mn}^{i}\kappa^{i-1}\left(\widetilde{\mathbf{R}}\mathbf{R}^{i-1}\widehat{\mathbf{y}}_m\right)^{\top}\widehat{\mathbf{x}}_n}_{\mathbf{Q}_{N,mn}^{i}}\Bigg),\end{aligned} \tag{17}$$

where i represents the current ith update, and $\mu_p^i = \widetilde{\mathbf{R}}\left(\mathbf{R}^{i-1}\mathbf{y}_m + \mathbf{t}^{i-1}\right) + \widetilde{\mathbf{t}}$.

For this optimization problem, we first need to acquire the gradient of $\mathbf{Q}(\Theta)$ in Eq. (17) w.r.t. $\boldsymbol{\xi}$ as follows,

$$\nabla\mathbf{Q}^{i} = \sum_{n=1}^{N}\sum_{m=1}^{M}\left(\nabla\mathbf{Q}_{P,mn}^{i} + \nabla\mathbf{Q}_{N,mn}^{i}\right), \tag{18}$$

where $\nabla\mathbf{Q}_{P,mn}^{i} = [\mathbf{J}^{i}_{\mathbf{Q}^{i}_{P,mn},\widetilde{\theta}}, \mathbf{J}^{i}_{\mathbf{Q}^{i}_{P,mn},\widetilde{\mathbf{t}}}]^{\top} \in \mathbb{R}^{6\times 1}$ and $\nabla\mathbf{Q}_{N,mn}^{i} = [\mathbf{J}^{i}_{\mathbf{Q}_{N,mn}}, \mathbf{0}_{1\times 3}]^{\top} \in \mathbb{R}^{6\times 1}$. It can be written as a 2×6 Jacobian matrix:

$$\begin{aligned}\mathbf{J}_{\mathbf{Q}_{mn}^{i},\boldsymbol{\xi}} = \begin{bmatrix} \mathbf{J}^{i}_{\mathbf{Q}^{i}_{P,mn},\widetilde{\theta}} & \mathbf{J}^{i}_{\mathbf{Q}^{i}_{P,mn},\widetilde{\mathbf{t}}} \\ \mathbf{J}^{i}_{\mathbf{Q}_{N,mn}} & \mathbf{0}_{1\times 3} \end{bmatrix} = \begin{bmatrix} \frac{\partial\mathbf{Q}_{P,mn}^{i}}{\partial\widetilde{\theta}_1} & & & & \\ \frac{\partial\mathbf{Q}_{N,mn}^{i}}{\partial\widetilde{\theta}_1} & & & & \\ \frac{\partial\mathbf{Q}_{P,mn}^{i}}{\partial\widetilde{\theta}_2} & \frac{\partial\mathbf{Q}_{P,mn}^{i}}{\partial\widetilde{\theta}_3} & \frac{\partial\mathbf{Q}_{N,mn}^{i}}{\partial\widetilde{t}_1} & \frac{\partial\mathbf{Q}_{N,mn}^{i}}{\partial\widetilde{t}_2} & \frac{\partial\mathbf{Q}_{N,mn}^{i}}{\partial\widetilde{t}_3} \\ \frac{\partial\mathbf{Q}_{N,mn}^{i}}{\partial\widetilde{\theta}_2} & \frac{\partial\mathbf{Q}_{N,mn}^{i}}{\partial\widetilde{\theta}_3} & 0 & 0 & 0 \end{bmatrix}\end{aligned} \tag{19}$$

Then we need to solve the above Jacobian matrix. From Eq. (16), we know that $\widetilde{\mathbf{R}}$ is a function of $\widetilde{\theta}$. Therefore, using the chain rule for matrix derivative [38], we can compute the items $\frac{\partial\mathbf{Q}_{P,mn}^{i}}{\partial\widetilde{\theta}_j}$ as follows:

$$\frac{\partial\mathbf{Q}_{P,mn}^{i}}{\partial\widetilde{\theta}_j} = \operatorname{tr}\left[\left(\frac{\partial\mathbf{Q}_{P,mn}^{i}}{\partial\widetilde{\mathbf{R}}}\right)^{\top}\frac{\partial\widetilde{\mathbf{R}}}{\partial\widetilde{\theta}_j}\right],\ j \in \{1,2,3\}$$

where

$$\begin{aligned}\frac{\partial\mathbf{Q}_{P,mn}^{i}}{\partial\widetilde{\mathbf{R}}} = \left(\mathbf{\Sigma}^{i-1}\right)^{-1}\cdot(-\mathbf{x}_n(\mathbf{I} + \widetilde{\mathbf{t}} + (\mathbf{R}^{i-1}\mathbf{y}_m + \mathbf{t}^{i-1})) \\ \cdot(\mathbf{R}^{i-1}\mathbf{y}_m + \mathbf{t}^{i-1})^{\top}),\end{aligned}$$

and $(\partial\widetilde{\mathbf{R}}/\partial\widetilde{\theta}_j)$ can be solved according to Rodrigues' rotation formula, which is presented in Appendix.C. Similarly, we can obtain:

$$\frac{\partial\mathbf{Q}_{P,mn}^{i}}{\partial\widetilde{t}_j} = \operatorname{tr}\left[\left(\frac{\partial\mathbf{Q}_{P,mn}^{i}}{\partial\widetilde{\mathbf{t}}}\right)^{\top}\frac{\partial\widetilde{\mathbf{t}}}{\partial\widetilde{t}_j}\right],\ j \in \{1,2,3\}$$

where

$$\frac{\partial\mathbf{Q}_{P,mn}^{i}}{\partial\widetilde{\mathbf{t}}} = (\mathbf{\Sigma}^{i-1})^{-1}(-\mathbf{x}_n + \widetilde{\mathbf{t}} + \widetilde{\mathbf{R}}(\mathbf{R}^{i-1}\mathbf{y}_m + \mathbf{t}^{i-1})),$$

and $(\partial\widetilde{\mathbf{t}}/\partial\widetilde{t}_j)$ is its corresponding unit base vector. Then, using the same method, we have:

$$\frac{\partial\mathbf{Q}_{N,mn}^{i}}{\partial\widetilde{\theta}_j} = -p_{mn}^{i}\kappa^{i-1}\operatorname{tr}\left[\mathbf{R}^{i-1}\widehat{\mathbf{y}}_m\widehat{\mathbf{x}}_n^{\top}\frac{\partial\widetilde{\mathbf{R}}}{\partial\widetilde{\theta}_j}\right].$$

After the gradient of $\mathbf{Q}(\Theta)$ has been computed, we can obtain the $\boldsymbol{\xi}$. Then the transformation $[\widetilde{\mathbf{R}}, \widetilde{\mathbf{t}}]$ can be solved using Eq. (16). Finally, we obtain the transformation at the ith update as follows:

$$\mathbf{R}^i = \widetilde{\mathbf{R}}\mathbf{R}^{i-1}, \quad \mathbf{t}^i = \widetilde{\mathbf{R}}\mathbf{t}^{i-1} + \widetilde{\mathbf{t}} \tag{20}$$

For the update of $\boldsymbol{\Sigma}$, after differentiating $\mathbf{F}(\Theta)$ regarding $\boldsymbol{\Sigma}$ and equating it to 0, we obtain:

$$\boldsymbol{\Sigma}^i = \frac{\sum_{n=1}^{N}\sum_{m=1}^{M} p_{mn}^i (\mathbf{x}_n - \mu_p^i)(\mathbf{x}_n - \mu_p^i)^\top}{N_{\mathbf{p}}^i}. \tag{21}$$

In the same way, let $\frac{\partial \mathbf{F}}{\partial \kappa} = 0$. The function w.r.t. κ is solved as follows:

$$-\frac{1}{\kappa} + \frac{e^{\kappa} + e^{-\kappa}}{e^{\kappa} - e^{-\kappa}} = \frac{1}{N_{\mathbf{P}}^i}\sum_{m=1}^{M}\sum_{n=1}^{N} p_{mn}^i \left(\mathbf{R}^i \widehat{\mathbf{y}}_m\right)^\top \widehat{\mathbf{x}}_n. \tag{22}$$

The closed-form solution of κ cannot be obtained from this nonlinear function. Therefore, we utilize the fixed-point iteration method to update its value.

Algorithm 1: Anisotropic Generalized Point Set Registration Based on VBI

Input: Point sets and corresponding normal vector sets $\mathbf{X}, \widehat{\mathbf{X}}, \mathbf{Y}, \widehat{\mathbf{Y}}$
Output: $\mathbf{R}^\star$ *and* $\mathbf{t}^\star$
Initialization: $\mathbf{R} = \mathbf{I}_3$, $\mathbf{t} = \mathbf{0}_{3\times 1}$, ω = 0.5, κ, λ, $\boldsymbol{\Sigma}$, $\langle \alpha_m \rangle = \frac{1}{M}$.
repeat
  VB E-step:
  -Update $\langle \alpha_m \rangle$, $\langle \varphi_{mn} \rangle$ and $\mathbf{P} = (p_{mn})$ by (10), (11) and (13) respectively;
  VB M-step:
  -Update $\mathbf{R}$ and $\mathbf{t}$ by (20);
  -Update $\boldsymbol{\Sigma}$ and κ by (21) and (22);
until *Convergence*;
return $\mathbf{R}^\star$ *and* $\mathbf{t}^\star$.

D. Implementation Details

The AGBCPD algorithm is summarized in Algorithm 1. Aside from the parameters that have been shown in Algorithm 1, the initial κ and $\boldsymbol{\Sigma}$ are set as κ = 10 and $\boldsymbol{\Sigma}$ = diag(100, 100, 100), respectively. This setup ensures the generality of the algorithm which means we suppose that the two PSs have a bad initial alignment. As the parameters are updated iteratively, κ will be larger, and $\boldsymbol{\Sigma}$ will be smaller. To ensure the calculability of κ, we empirically limit the maximum value of κ to 50 during the algorithm's iterations. The λ is set as infinity which is the same as the BCPD. The following conditions are used to conclude whether the method converges: 1) $\mathrm{tr}(\boldsymbol{\Sigma})/3$ is less than 10^{-3}; 2) the difference $\Delta\mathrm{tr}(\boldsymbol{\Sigma})/3$ between two successive iterations is less than 10^{-5}; 2) the maximum iterations are 100. All algorithms are developed using MATLAB.

IV. Experimental Results and Discussion

A. Dataset Preparation and Evaluation Metrics

Two sets of experiments, referred to as *full-to-full* and *partial-to-full* cases, are conducted to validate the registration accuracy and robustness of our algorithm. In computer-assisted surgery (CAS), the *source* PS $\mathbf{Y}$ includes M = 1568 points and is reconstructed from the computed tomography (CT) of a human pelvis or femur bone as shown in Fig.1. The corresponding normal vector set $\widehat{\mathbf{Y}}$ is generated using the PlanePCA method [39]. PlanePCA is to perform the principal component analysis (PCA) of an augmented data matrix that consists of one positional point and its neighbors [39]. Then the principal component with the smallest variance is chosen as the normal vectors. The $N_{\text{inliers}} = 100$ inlier intra-operative target PSs $(\mathbf{X}, \widehat{\mathbf{X}})$ are randomly sampled from $(\mathbf{Y}, \widehat{\mathbf{Y}})$. For each set of experiments, two different types of zero-mean Gaussian positional noise are added to $\mathbf{X}$ respectively: 1) isotropic positional noise with the covariance matrix $\boldsymbol{\Sigma}_{iso} = \mathbf{I}_{3\times 3}$; 2) anisotropic positional noise with the covariance matrix

$$\boldsymbol{\Sigma}_{ani} = \mathbf{diag}(1/11, 1/11, 9/11). \tag{23}$$

For the orientation error in two groups, we use the same 1° standard deviation to produce the orientation noise, e.g., $\kappa = 3200$ [40], which are then injected into $\widehat{\mathbf{X}}$. Then, five different ratios of outliers from 10% to 90% with an interval of 20% are added to $(\mathbf{X}, \widehat{\mathbf{X}})$ to generate the *disturbed* $(\mathbf{X}, \widehat{\mathbf{X}})$. The positional vectors with outliers are produced by applying a displacement vector uniformly sampled within $[20\text{mm}, 30\text{mm}]$ to the randomly sampled points from $\mathbf{Y}$. The normal vectors associated with outliers are randomly generated within $[0^\circ, 360^\circ]$. Then we obtain the final *disturbed* $(\mathbf{X}, \widehat{\mathbf{X}})$ with $N = 110$ to 190.

In each registration trial, the ground-truth values of rigid transformation matrix $[\mathbf{R_{true}}, \mathbf{t_{true}}]$ is randomly generated from $[10^\circ, 25^\circ]$ and $[10\text{mm}, 25\text{mm}]$. [1] Then the source PS $(\mathbf{Y}, \widehat{\mathbf{Y}})$ are misaligned by applying the real $[\mathbf{R_{true}}, \mathbf{t_{true}}]$ to $(\mathbf{Y}, \widehat{\mathbf{Y}})$, denoted as the *misaligned* $(\mathbf{Y}, \widehat{\mathbf{Y}})$. In all experiments, *disturbed* $(\mathbf{X}, \widehat{\mathbf{X}})$ and *misaligned* $(\mathbf{Y}, \widehat{\mathbf{Y}})$ are registered, after which the rigid transformation matrix $\mathbf{R}_{cal}$ and $\mathbf{t}_{cal}$ are acquired. We conduct $N_{\text{trial}} = 100$ registration trials in each specific case of rigid transformation matrix and noise type to further get the error statistics (e.g., mean and standard deviation).

The rotation and translation error values in each registration trial are computed to evaluate the registration performances. The statistics including the mean and standard deviation are further computed with the N_{trial} error values and reported. We compute and process the error values of N_{trial} registration trials in each case. In one specific registration trial, the rotation and translation error values are defined as follows:

$$\text{Error}_{\text{Rot}} = \arccos\left[\frac{\mathrm{tr}\left(\mathbf{R_{true}}\mathbf{R}_{cal}^\top\right) - 1}{2}\right] \times \frac{180^\circ}{\pi} \tag{24}$$

[1]Note that our method focuses on improving the performance of the local registration approaches, which assumes the coarse registration has been done using the anatomical landmarks in the surgical scenario. Therefore, the deviation angle and distance are reasonably not very large.

TABLE I
ROTATION AND TRANSLATION ERRORS UNDER ISOTROPIC AND ANISOTROPIC NOISE. DIFFERENT OUTLIER RATIOS ARE ADDED TO $(\mathbf{X}, \widehat{\mathbf{X}})$. THE PELVIS MODEL IS CHOSEN IN THIS SERIES OF EXPERIMENTS.

Error Type	Outliers' Percents	10%	30%	50%	70%	90%	10%	30%	50%	70%	90%
	Noise type / Methods	Isotropic Noise					Anisotropic Noise				
Rot (°)	ICP [18]	1.0916	1.4291	1.6023	1.6663	1.9720	0.6201	1.2770	1.4827	1.7745	1.7631
	CPD [12]	0.7563	0.6628	0.6589	1.2986	2.0406	0.2468	0.2443	0.4078	1.4165	2.1207
	BCPD [27]	2.0070	1.3074	1.3672	1.5057	1.4941	1.0188	1.1445	1.2737	1.6637	1.4385
	IGBCPD	0.5815	**0.4925**	**0.4595**	**0.4275**	0.5445	0.2413	0.4046	0.3631	0.2423	0.4428
	AGBCPD	**0.5501**	0.5268	0.4885	0.5288	**0.5278**	**0.1965**	**0.1512**	**0.1828**	**0.1911**	**0.1579**
Trans (mm)	ICP [18]	0.8204	1.1200	1.2586	1.3810	1.5555	0.4528	1.0660	1.0903	1.5267	1.4029
	CPD [12]	2.9234	2.8929	3.3056	3.5889	3.9524	3.2185	3.1238	3.2820	3.5479	3.8742
	BCPD [27]	3.3070	3.4101	3.2869	3.2570	3.4621	3.3063	3.2344	3.3332	3.3730	3.4659
	IGBCPD	0.5935	0.5423	0.5248	0.5815	**0.5266**	0.2614	0.3774	0.3439	0.2739	0.4190
	AGBCPD	**0.5745**	**0.5137**	**0.5116**	**0.5451**	0.5645	**0.2419**	**0.2591**	**0.2293**	**0.2090**	**0.2232**

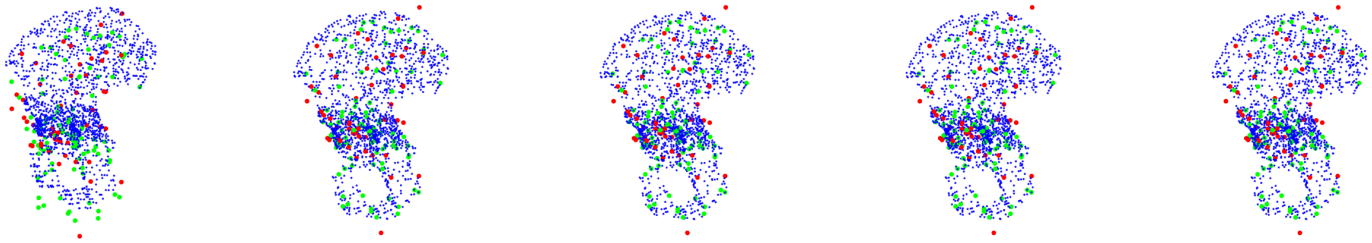

Fig. 2. Registration process using our AGBCPD method with 70% outliers and anisotropic positional noise. (a)~(d): the registration result before registration, 5th, 10th and 100th iteration using the proposed method, respectively; (e): ground truth. Blue, green, and red PSs indicate the source PS Y, the target PS X, and outliers respectively.

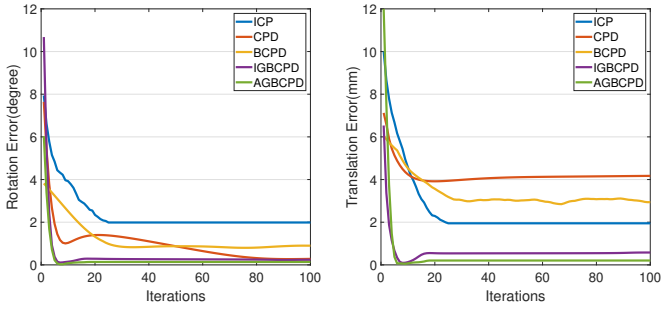

Fig. 3. Convergence speed of five methods with respect to the iterations. Anisotropic positional noise and 70% outliers are chosen. Left: rotation error. Right: translation error.

$$\text{Error}_{\text{Trans}} = \|\mathbf{t}_{cal} - \mathbf{t}_{\mathbf{true}}\|_2 \tag{25}$$

where tr(•) represents the trace of a matrix, $||\bullet||_2$ denotes the L2-norm.

B. Full-to-Full Registration

In this set of experiments, the registration problems are in a full-to-full manner, which means that $(\mathbf{X}, \widehat{\mathbf{X}})$ are randomly sampled from the whole CT model of pelvis and femur bones. We compare our method (i.e., AGBCPD) against three registration methods including: ICP [18], CPD [12], BCPD [27]. Furthermore, ablating the assumption of anisotropic positional noise, we build and test the isotropic GBCPD (IGBCPD) as an ablation study. Compared with AGBCPD, the difference is that IGBCPD uses equal isotropic covariances σ^2 to replace the anisotropic covariance matrix $\mathbf{\Sigma}$ in the probability density function Eq. (3) of HMM like the isotropic assumption in CPD.

1) Pelvis Model: As shown in Table I, (1) our two GBCPD variants outperform the other three methods in all tests under isotropic positional noise while the rotation and translation errors are very similar for both AGBCPD and IGBCPD; (2) for anisotropic positional noise, AGBCPD has the smallest rotation and translation errors, and it still maintains good robustness with the increase of outliers, while the other four methods do not.

Fig. 2 shows the registration process for different iterations on the human pelvis model. It presents the registration results using the AGBCPD method in the 0th (before registration), 5th, 10th, 100th iteration. As shown in Fig. 2, the result in the 10th iteration has little difference from the final 100th iteration, which means our method can achieve fast convergence speed.

Furthermore, we quantitatively compare the convergence speed of these five methods with respect to the iterations in the same conditions. As shown in Fig. 3, under anisotropic noise and 70% outliers, the convergence speeds of our two GBCPD methods are faster than the other three methods. In addition, our AGBCPD method achieves the smallest errors, which also demonstrates that AGBCPD is insusceptible to anisotropic noise and outliers.

TABLE II
ROTATION AND TRANSLATION ERRORS UNDER ISOTROPIC AND ANISOTROPIC NOISE. DIFFERENT OUTLIER RATIOS ARE ADDED TO $(\mathbf{X}, \widehat{\mathbf{X}})$. THE FEMUR MODEL IS CHOSEN IN THIS SERIES OF EXPERIMENTS.

Error Type	Outliers' Percents	10%	30%	50%	70%	90%	10%	30%	50%	70%	90%
	Noise type / Methods	Isotropic Noise					Anisotropic Noise				
Rot (°)	ICP [18]	2.6877	3.9594	4.8543	5.3575	5.2281	2.0556	3.1001	4.5424	4.6535	4.6680
	CPD [12]	1.5168	1.1783	1.8922	3.9650	5.3339	0.2909	0.6374	1.6639	4.0521	4.7526
	BCPD [27]	1.6861	1.0474	2.8246	3.4831	3.4021	1.8640	1.6205	2.8059	3.2267	3.5296
	IGBCPD	0.9530	1.0353	1.1096	**0.9228**	1.1005	0.3624	0.3586	0.4056	0.3391	0.4437
	AGBCPD	**0.9523**	**0.8310**	**1.0660**	0.9795	**0.9304**	**0.2759**	**0.3204**	**0.3670**	**0.3093**	**0.2792**
Trans (mm)	ICP [18]	1.0479	1.6958	1.8395	2.1533	2.0304	0.9169	1.4334	1.8280	1.9296	1.7418
	CPD [12]	3.3426	3.3414	3.5482	3.8305	4.0380	2.9218	3.1019	3.6909	3.9698	4.0524
	BCPD [27]	3.2149	3.1210	3.3414	3.2779	3.4497	2.7982	3.0110	3.7082	3.4451	3.1228
	IGBCPD	0.4804	0.5228	0.5204	0.5633	**0.4781**	0.3008	0.2624	0.3060	0.2837	0.3241
	AGBCPD	**0.4526**	**0.5171**	**0.5147**	**0.4974**	0.4981	**0.2521**	**0.2445**	**0.2021**	**0.2263**	**0.2119**

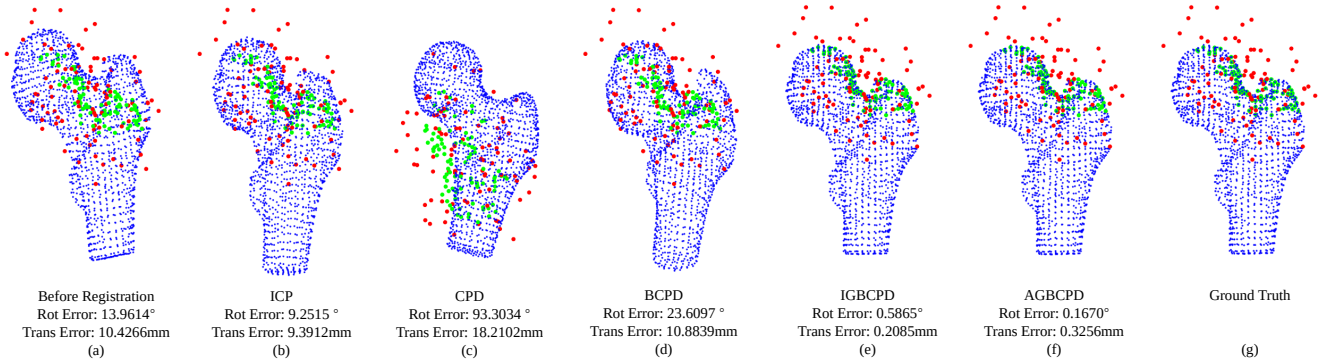

Fig. 4. Subfigure (a) represents the result before the registration. Subfigures (b)~(f) represent five registration results using ICP, CPD, BCPD, IGBCPD, and our AGBCPD method respectively. Subfigure (g) is the ground truth. Anisotropic noise and 90% outliers are added into PS $(\mathbf{X}, \widehat{\mathbf{X}})$. Blue, green, and red PSs indicate the source PS, the target PS, and outliers respectively.

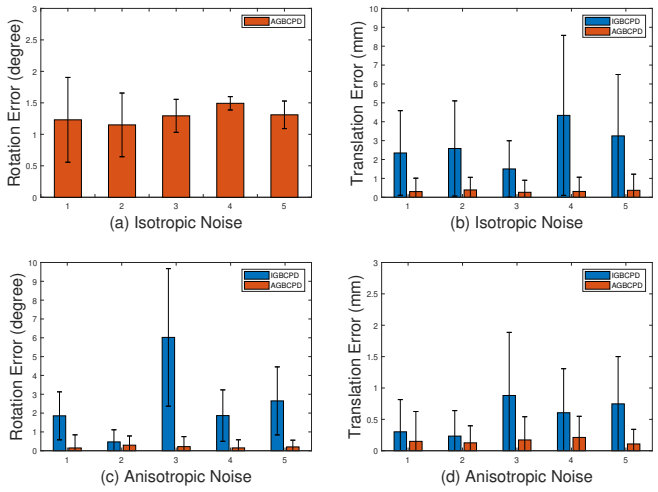

Fig. 5. Mean and standard deviation (std) of rotation and translation error using AGBCPD & IGBCPD with different noises. (a) and (b) is under the isotropic positional noise; (c) and (d) is under the anisotropic positional noise.

2) Femur Model: Table II shows the corresponding quantitative results in the femur model. As shown in Table II, both IGBCPD and AGBCPD have a better performance than other methods in all cases, which benefit from the incorporated normal vectors. It should also be noted that AGBCPD demonstrates significant advantages compared with others including IGBCPD, especially in the case of anisotropic positional noise.

Moreover, we use the ***ttest*** function in MATLAB to compute the p-value of our proposed methods compared with other methods in both pelvis and femur tests. Almost all p-values are within 0.05 significance level, which proves that the difference between AGBCPD and other methods is statistically significant.

C. Partial-to-Full Registration

In real-world surgical scenarios, such as total hip replacement (THR) surgery, the intra-operative points usually concentrate in the proximal femur head while the femur includes the region distal to the lesser trochanter, femur head, and femur neck, as shown in Fig. 4(g). This region is small compared with the whole preoperative femur model. Therefore, the registrations are partial to full.

Fig. 4 shows the qualitative results with 90% outliers and anisotropic noise injected. As shown in Fig. 4, the two PSs are successfully registered with AGBCPD, while IGBCPD also has an acceptable performance. However, other methods fail to align the *partial* intraoperative points $(\mathbf{X}, \widehat{\mathbf{X}})$ (i.e., green points) with the *full* preoperative PS $(\mathbf{Y}, \widehat{\mathbf{Y}})$ (i.e., blue points). Therefore, in *partial-to-full* registration, ICP, CPD, and BCPD are not included in the quantitative analysis.

Fig. 5 shows the quantitative results in *partial-to-full registration*[2]. As shown in Fig. 5, in all cases, AGBCPD achieves both smaller rotation and translation error values than IGBCPD. Compared with the full-to-full case, the difference in the partial-to-full case between two GBCPD methods becomes bigger, which proves our anisotropic model AGBCPD can deal with more complex and difficult scenarios and keep robust and accurate.

D. Discussion

This paper generalizes the recently proposed Bayesian Coherent Point Drift (BCPD) method to the six-dimensional scenario. The proposed noise model is decomposed into three parts to be solved alternately: the membership probability of mixture distributions, the soft correspondence estimation, and the model parameters (i.e., the rotation matrix, translation vector, the covariance matrix with the anisotropic positional error, and the concentration parameter with the estimation of the normal vectors). Especially, the convergence is guaranteed at the theoretical level using the variational inference theory.

To summarize, the experimental results demonstrate that our AGBCPD method outperforms other algorithms in the following points: (a) convergence speed; (b) robustness and stability to noise, outliers, and incomplete partial data; (c) registration accuracy. Especially, the comparison between IGBCPD and AGBCPD proves the correctness and effectiveness of the more generalized assumption about the anisotropic positional noise. It is common that the positional noise is anisotropic in many CAS applications. For example, the standard deviation of the reflective marker localization error in the line-of-sight direction of an optical tracking device (e.g. NDI's Polaris Vega) is 3 or 5 times than those in the other two orthogonal directions [34]. Our anisotropic model can deal with these actual surgical applications.

In terms of orthopedic surgery, our experimental results in partial-to-full registration demonstrated that our proposed method can achieve the high accuracy requirement in surgical scenarios. More importantly, the proposed method is quite robust to increasing percentages of outliers.

Limitations: We expect that this study can motivate more progressive PSR methods that consider the anisotropic cases and orientational features (i.e., normal vectors). There are still several limitations in our AGBCPD method. First, the source PS $\mathbf{Y}$ and corresponding normal vector set $\widehat{\mathbf{Y}}$ is defined as an ideal point set without noise, while the target PS is assumed to be generated from the source PSs. To extend the perfect assumption, we can assume both source and target PSs with noise are generated from probabilistic models. Second, the proposed method doesn't utilize the local structures among adjacent points which can help to estimate the correspondences [41]. In practice, it is effortless to incorporate the AGBCPD method into these algorithms that consider the features of local structures. Third, because of the complicated consideration of the anisotropic noise and orientational features, the AGBCPD takes more time than the original BCPD in one iteration, although it has the fastest convergence speed of these five methods with respect to the iterations in the same conditions as shown in Fig. 3.

[2]The rotation error values obtained when using IGBCPD with isotropic noise reach 21° with a standard deviation of 43°. These values are therefore not shown in Fig. 5(a).

V. Conclusions

In this work, we present a robust and accurate rigid point set registration (RPSR) method under the variational bayesian inference (VBI) framework, where both the positional and normal vectors are used while the anisotropic positional noise is considered. Experimental results demonstrate its great clinical values for computer-assisted surgery (CAS). The presented work can be further improved in the following two aspects. First, the prior distributions over $\mathbf{\Sigma}$, κ, or the variables $\mathbf{R}, \mathbf{t}$ can be introduced to potentially make the generative model more accurate [36]. Second, several ways to accelerate the complex model will be explored [42].

Appendices

A. vMF Distribution

We choose the vMF distribution to represent the orientational feature in multi-dimension data [43]. It's a common and simple parametric distribution for directional data which is parametrized by the mean direction $\boldsymbol{\mu}_o$ and the concentration $\boldsymbol{\kappa}$. The PDF of the vMF distribution for d-dimensional unit directional feature $\widehat{\mathbf{x}}_n$ is defined as:

$$p(\widehat{\mathbf{x}}_n \mid \boldsymbol{\mu}_o, \boldsymbol{\kappa}) = Z(\kappa) e^{\kappa \boldsymbol{\mu}_o^\top \widehat{\mathbf{x}}_n},$$

where $\kappa \geq 0,\ ||\boldsymbol{\mu}_o|| = 1$, and $Z(\kappa)$ is the normalizer of the vMF distribution as follows:

$$Z(\kappa) = (2\pi)^{-d/2} \frac{\kappa^{d/2-1}}{I_{d/2-1}(\kappa)},$$

where $d \geq 2$ and $I_{d/2-1}(\bullet)$ is the modified Bessel function of the first kind of order $(d/2-1)$. In this paper, the directional data are three-dimensional normal vectors, *i.e.* $d = 3$. Then we have

$$\frac{\kappa^{1/2}}{I_{1/2}(\kappa)} = \sqrt{\frac{\pi}{2}} \frac{\kappa}{\sinh \kappa},\ \ \sinh \kappa = \frac{1}{2}(e^{\kappa} - e^{-\kappa}).$$

Substituting these two equations into $Z(\kappa)$, we can obtain:

$$Z(\kappa) = \frac{\kappa}{4\pi \sinh \kappa} = \frac{\kappa}{2\pi \left(e^{\kappa} - e^{-\kappa}\right)}.$$

The concentration of the distribution about the mean direction $\boldsymbol{\mu}_o$ will be higher with increasing concentration κ.

B. Derivation of Eq. (14)

To simplify writing, we denote $x = (\mathbf{X}, \widehat{\mathbf{X}}), y = (\mathbf{Y}, \widehat{\mathbf{Y}}), \theta_{12} = (\alpha, c, v), \theta_3 = (\mathbf{R}, \mathbf{t}, \mathbf{\Sigma}^2, \kappa)$. Given $q(\theta_{12})$, we have:

$$\begin{aligned}
\mathcal{L}(q) &= \int q(\theta) \cdot \ln \frac{p(x,y,\theta)}{q(\theta)} d\theta \\
&= \int q\left(\theta_{12}, \theta_3\right) \ln \frac{p\left(x, y, \theta_{12}, \theta_3\right)}{q\left(\theta_{12}\right)} d\theta_{12} d\theta_3 \\
&\quad - \int q\left(\theta_1 \theta_2\right) q(\theta_3) \ln q(\theta_3) d\theta_{12} d\theta_3 \\
&= \int q(\theta_3) E_{q(\theta_{12})}[\ln p(x,y,\theta_{12},\theta_3)] d\theta_3 \\
&\quad - E_{q(\theta_{12})}\left[\ln q\left(\theta_{12}\right)\right] - \int q(\theta_3) \ln q(\theta_3) d\theta_3 \\
&= \int q(\theta_3) E_{q(\theta_{12})}[\ln p(x,y,\theta_{12},\theta_3)] d\theta_3 \\
&\quad - \int q(\theta_3) \ln q(\theta_3) d\theta_3 + const,
\end{aligned} \tag{26}$$

Because $q_3\left(\theta_3\right)$ is a Dirac delta function, we can drop the entropy term $-\int q(\theta_3) \ln q(\theta_3) d\theta_3$. Then we obtain the form of Eq. (14).

C. Derivation of $\frac{\partial \widetilde{\mathbf{R}}}{\partial \widetilde{\theta}_j}$

$$\begin{aligned}
\frac{\partial \widetilde{\mathbf{R}}}{\partial \widetilde{\theta}_j} =& \frac{\partial \frac{sin(\|\widetilde{\theta}\|)}{\|\widetilde{\theta}\|}}{\partial \widetilde{\theta}_j} [\widetilde{\theta}]_\times + \frac{sin(\|\widetilde{\theta}\|)}{\|\widetilde{\theta}\|} \frac{\partial [\widetilde{\theta}]_\times}{\partial \widetilde{\theta}_j} \\
&+ \frac{\partial \frac{1-cos(\|\widetilde{\theta}\|)}{\|\widetilde{\theta}\|^2}}{\partial \widetilde{\theta}_j} [\widetilde{\theta}]_\times^2 + \frac{1-cos(\|\widetilde{\theta}\|)}{\|\widetilde{\theta}\|^2} \frac{\partial [\widetilde{\theta}]_\times^2}{\partial \widetilde{\theta}_j}, \\
& j \in \{1,2,3\}.
\end{aligned} \tag{27}$$

REFERENCES

[1] L. Li, M. Yang, L. Weng, and C. Wang, "Robust localization for intelligent vehicles based on pole-like features using the point cloud," *IEEE Transactions on Automation Science and Engineering*, 2021.

[2] L. Li, S. Bano, J. Deprest, A. L. David, D. Stoyanov, and F. Vasconcelos, "Globally optimal fetoscopic mosaicking based on pose graph optimisation with affine constraints," *IEEE Robotics and Automation Letters*, vol. 6, no. 4, pp. 7831–7838, 2021.

[3] K. Wu, Z. J. Daruwalla, K. L. Wong, D. Murphy, and H. Ren, "Development and selection of asian-specific humeral implants based on statistical atlas: toward planning minimally invasive surgery," *International journal of computer assisted radiology and surgery*, vol. 10, no. 8, pp. 1333–1345, 2015.

[4] J. Wu, M. Liu, Y. Huang, C. Jin, Y. Wu, and C. Yu, "Se (n)++: An efficient solution to multiple pose estimation problems," *IEEE Transactions on Cybernetics*, 2020.

[5] F. Pomerleau, F. Colas, and R. Siegwart, "A review of point cloud registration algorithms for mobile robotics," *Foundations and Trends in Robotics*, vol. 4, no. 1, pp. 1–104, 2015.

[6] L. Han, L. Xu, D. Bobkov, E. Steinbach, and L. Fang, "Real-time global registration for globally consistent rgb-d slam," *IEEE Transactions on Robotics*, vol. 35, no. 2, pp. 498–508, 2019.

[7] A. L. Fuhrmann, R. Splechtna, and J. Přikryl, "Comprehensive calibration and registration procedures for augmented reality," in *Immersive Projection Technology and Virtual Environments 2001*. Springer, 2001, pp. 219–227.

[8] L. Qian, J. Y. Wu, S. P. DiMaio, N. Navab, and P. Kazanzides, "A review of augmented reality in robotic-assisted surgery," *IEEE Transactions on Medical Robotics and Bionics*, vol. 2, no. 1, pp. 1–16, 2019.

[9] A. Brounstein, I. Hacihaliloglu, P. Guy, A. Hodgson, and R. Abugharbieh, "Towards real-time 3d us to ct bone image registration using phase and curvature feature based gmm matching," in *International Conference on Medical Image Computing and Computer-Assisted Intervention*. Springer, 2011, pp. 235–242.

[10] T. Vercauteren, M. Unberath, N. Padoy, and N. Navab, "Cai4cai: The rise of contextual artificial intelligence in computer-assisted interventions," *Proceedings of the IEEE*, vol. 108, no. 1, pp. 198–214, 2019.

[11] M. Ciganovic, F. Ozdemir, F. Pean, P. Fuernstahl, C. Tanner, and O. Goksel, "Registration of 3d freehand ultrasound to a bone model for orthopedic procedures of the forearm," *International journal of computer assisted radiology and surgery*, vol. 13, no. 6, pp. 827–836, 2018.

[12] A. Myronenko and X. Song, "Point set registration: Coherent point drift," *IEEE transactions on pattern analysis and machine intelligence*, vol. 32, no. 12, pp. 2262–2275, 2010.

[13] J. Ma, W. Qiu, J. Zhao, Y. Ma, A. L. Yuille, and Z. Tu, "Robust $l\_\{2\}e$ estimation of transformation for non-rigid registration," *IEEE Transactions on Signal Processing*, vol. 63, no. 5, pp. 1115–1129, 2015.

[14] L. Bai, X. Yang, and H. Gao, "Nonrigid point set registration by preserving local connectivity," *IEEE transactions on cybernetics*, vol. 48, no. 3, pp. 826–835, 2017.

[15] J. Ma, J. Zhao, J. Jiang, H. Zhou, and X. Guo, "Locality preserving matching," *International Journal of Computer Vision*, vol. 127, no. 5, pp. 512–531, 2019.

[16] J. Ma, X. Jiang, J. Jiang, J. Zhao, and X. Guo, "Lmr: Learning a two-class classifier for mismatch removal," *IEEE Transactions on Image Processing*, vol. 28, no. 8, pp. 4045–4059, 2019.

[17] J. Ma, Y. Ma, and C. Li, "Infrared and visible image fusion methods and applications: a survey," *Information Fusion*, vol. 45, pp. 153–178, 2019.

[18] P. J. Besl and N. D. McKay, "Method for registration of 3-d shapes," in *Sensor fusion IV: control paradigms and data structures*, vol. 1611. International Society for Optics and Photonics, 1992, pp. 586–606.

[19] J. Zhang, Y. Yao, and B. Deng, "Fast and robust iterative closest point," *IEEE Transactions on Pattern Analysis and Machine Intelligence*, 2021.

[20] J. Yang, H. Li, D. Campbell, and Y. Jia, "Go-icp: A globally optimal solution to 3d icp point-set registration," *IEEE transactions on pattern analysis and machine intelligence*, vol. 38, no. 11, pp. 2241–2254, 2015.

[21] S. Bouaziz, A. Tagliasacchi, and M. Pauly, "Sparse iterative closest point," in *Computer graphics forum*, vol. 32, no. 5. Wiley Online Library, 2013, pp. 113–123.

[22] Y. Yang, D. Fan, S. Du, M. Wang, B. Chen, and Y. Gao, "Point set registration with similarity and affine transformations based on bidirectional kmpe loss," *IEEE transactions on cybernetics*, 2019.

[23] L. Maier-Hein, A. M. Franz, T. R. dos Santos, M. Schmidt, M. Fangerau, H.-P. Meinzer, and J. M. Fitzpatrick, "Convergent iterative closest-point algorithm to accomodate anisotropic and inhomogenous localization error," *IEEE Transactions on Pattern Analysis and Machine Intelligence*, vol. 8, no. 34, pp. 1520–1532, 2012.

[24] J. Ma, X. Jiang, A. Fan, J. Jiang, and J. Yan, "Image matching from handcrafted to deep features: A survey," *International Journal of Computer Vision*, vol. 129, no. 1, pp. 23–79, 2021.

[25] L. Li, M. Yang, C. Wang, and B. Wang, "Robust point set registration using signature quadratic form distance," *IEEE transactions on cybernetics*, vol. 50, no. 5, pp. 2097–2109, 2018.

[26] G. D. Evangelidis and R. Horaud, "Joint alignment of multiple point sets with batch and incremental expectation-maximization," *IEEE transactions on pattern analysis and machine intelligence*, vol. 40, no. 6, pp. 1397–1410, 2017.

[27] O. Hirose, "A bayesian formulation of coherent point drift," *IEEE transactions on pattern analysis and machine intelligence*, 2020.

[28] Y. Wang, Y. Sun, Z. Liu, S. E. Sarma, M. M. Bronstein, and J. M. Solomon, "Dynamic graph cnn for learning on point clouds," *Acm Transactions On Graphics (tog)*, vol. 38, no. 5, pp. 1–12, 2019.

[29] C. R. Qi, H. Su, K. Mo, and L. J. Guibas, "Pointnet: Deep learning on point sets for 3d classification and segmentation," in *Proceedings of the IEEE conference on computer vision and pattern recognition*, 2017, pp. 652–660.

[30] H. Yang, J. Shi, and L. Carlone, "Teaser: Fast and certifiable point cloud registration," *IEEE Transactions on Robotics*, 2020.

[31] Y. Wang and J. Solomon, "Prnet: Self-supervised learning for partial-to-partial registration," *NeurIPS*, 2019.

[32] C. Choy, W. Dong, and V. Koltun, "Deep global registration," in *Proceedings of the IEEE/CVF conference on computer vision and pattern recognition*, 2020, pp. 2514–2523.

[33] Z. Deng, Y. Yao, B. Deng, and J. Zhang, "A robust loss for point cloud registration," in *Proceedings of the IEEE/CVF International Conference on Computer Vision*, 2021, pp. 6138–6147.

[34] Z. Min and M. Q.-H. Meng, "General first-order target registration error model considering a coordinate reference frame in an image-guided surgical system," *Medical & Biological Engineering & Computing*, vol. 58, no. 12, pp. 2989–3002, 2020.

[35] Z. Min, H. Ren, and M. Q.-H. Meng, "Statistical model of total target registration error in image-guided surgery," *IEEE Transactions on Automation Science and Engineering*, vol. 17, no. 1, pp. 151–165, 2019.

[36] C. M. Bishop, *Pattern recognition and machine learning*. springer, 2006.

[37] J. Bernardo, M. Bayarri, J. Berger, A. Dawid, D. Heckerman, A. Smith, M. West *et al.*, "The variational bayesian em algorithm for incomplete data: with application to scoring graphical model structures," *Bayesian statistics*, vol. 7, no. 453-464, p. 210, 2003.

[38] K. B. Petersen, M. S. Pedersen *et al.*, "The matrix cookbook," *Technical University of Denmark*, vol. 7, no. 15, p. 510, 2008.

[39] K. Jordan and P. Mordohai, "A quantitative evaluation of surface normal estimation in point clouds," in *2014 IEEE/RSJ International Conference on Intelligent Robots and Systems*. IEEE, 2014, pp. 4220–4226.

[40] S. Billings and R. Taylor, "Generalized iterative most likely oriented-point (g-imlop) registration," *International journal of computer assisted radiology and surgery*, vol. 10, no. 8, pp. 1213–1226, 2015.

[41] J. Ma, J. Zhao, and A. L. Yuille, "Non-rigid point set registration by preserving global and local structures," *IEEE Transactions on image Processing*, vol. 25, no. 1, pp. 53–64, 2015.

[42] O. Hirose, "Acceleration of non-rigid point set registration with down-sampling and gaussian process regression," *IEEE Transactions on Pattern Analysis and Machine Intelligence*, vol. 43, no. 8, pp. 2858–2865, 2020.

[43] A. Banerjee, I. S. Dhillon, J. Ghosh, S. Sra, and G. Ridgeway, "Clustering on the unit hypersphere using von mises-fisher distributions." *Journal of Machine Learning Research*, vol. 6, no. 9, 2005.

Ang Zhang (Member, IEEE) received the B.E. degree in automation from Shandong University, Jinan, China, in 2015.

He is currently pursuing the Ph.D. degree at the Department of Electronic Engineering, The Chinese University of Hong Kong, Hong Kong. His current research interests include augmented reality, surgical navigation, and medical robotics.

Zhe Min (Member, IEEE) received the Ph.D. degree in Electronic Engineering from the Chinese University of Hong Kong (CUHK), Hong Kong, China, in 2019. Afterwards, he was a Postdoc Fellow at the Department of Electronic Engineering in CUHK, Hong Kong. He is now a Research Fellow with Centre for Medical Image Computing and Wellcome/EPSRC Centre for Interventional and Surgical Sciences, University College London, London, UK.

He serves as an Associate Editor for IEEE Robotics and Automation Letters (RA-L).

Zhengyan Zhang received the B.E. degree in Measurement and Control Technology and Instrumentation from Nanjing Tech University, Nanjing, China, in 2020.

He is currently pursuing the Master degree with the Department of Control Science and Engineering, Harbin Institute of Technology, Shenzhen, China. His current research interests include surgical navigation, augmented reality and medical image registration.

Xing Yang received the B.E. degree in mechanical and electronic engineering from Shandong University of Science and Technology, Shandong, China, in 2012 and the M.E. degree in mechanical and electronic engineering from North University of China, Taiyuan, China, in 2016. From June 2014 to May 2016, he was a joint student in Ningbo Institute of Materials Technology & Engineering, Chinese Academy of Sciences and his research field was mobile robot's location and navigation.

He is currently pursuing the Ph.D. of mechanical engineering in Harbin Institute of Technology, Shenzhen. His research interests include surgical robotics and continuum robotics.

Max Q.-H. Meng (M'92-F'07) received the Ph.D. degree in electrical and computer engineering from the University of Victoria, Victoria, BC, Canada, in 1992.

He is now a Professor and Chairman of the Department of Electronic and Electrical Engineering of the Southern University of Science and Technology in Shenzhen, China, on leave from the Department of Electronic Engineering, The Chinese University of Hong Kong, Hong Kong, and also with the Shenzhen Research Institute of the Chinese University of Hong Kong in Shenzhen, China. He has been a Professor of electronic engineering with the Chinese University of Hong Kong (CUHK), Hong Kong, since 2002, after being the Director of the ART (Advanced Robotics and Teleoperation) Lab and Professor for ten years with the Department of Electrical and Computer Engineering, University of Alberta, Edmonton, AB, Canada. He has authored over 500 journal and conference papers.

His current research interests include robotics, perception and sensing, human robot interaction, active medical devices, biosensors and sensor networks, and adaptive and intelligent systems. Prof. Meng is an Elected Member of the Administrative Committee of the IEEE Robotics and Automation Society and has served on many editorial boards. He is a recipient of the IEEE Millennium Medal, a Fellow of IEEE, a Fellow of Hong Kong Institution of Engineers, and a Fellow of the Canadian Academy of Engineering.